Microwave-free magnetometry based on cross-relaxation resonances in diamond nitrogen-vacancy centers

Rinat Akhmedzhanov,* Lev Gushchin, Nikolay Nizov, Vladimir Nizov, Dmitry Sobgayda, and Ilya Zelensky
Institute of Applied Physics of the Russian Academy of Sciences, 603950 Nizhny Novgorod, Russia

Philip Hemmer
Electrical & Computer Engineering Department, Texas A&M University, College Station, Texas 77843, USA
(Received 16 May 2017; published 6 July 2017)

We study cross-relaxation resonances between differently oriented groups of nitrogen-vacancy (NV) centers at small external magnetic fields. These resonances are observed using resonant optical pumping on the NV-center zero phonon line. We suggest a magnetometry protocol that is based on measuring the positions of cross-relaxation resonances on the fluorescence scan. This protocol does not require microwave radiation and can be used to find all components of the unknown magnetic field vector. A room-temperature variant of the protocol with off-resonant optical pumping is also briefly discussed.

DOI: 10.1103/PhysRevA.96.013806

I. INTRODUCTION

Negatively charged nitrogen-vacancy (NV) centers in diamond have been studied extensively over the last few years for multiple potential applications including quantum information processing [1], hybrid quantum systems [2], temperature [3], and magnetic sensing [4] and imaging [5]. Magnetic sensing with NV centers is commonly done using the optically detected magnetic resonance (ODMR) technique [4,6,7]. This technique involves probing the ground-state transitions of the negatively charged NV center with tunable microwave (MW) radiation. The resulting change in the ground-state population caused by the resonant MW radiation can be read out by observing changes in the level of photoluminescence induced by the laser pump (usually off-resonant). This approach can be used at temperatures ranging from cryogenic [8,9] to 700 K [10]. The feasibility of using both single defects and ensembles makes it possible to achieve the combination of spatial resolution and magnetic sensitivity appropriate for the task at hand. However, this approach also has some important limitations. The strong MW radiation required for the protocol cannot be applied near magnetic and conductive materials. In addition, optically off-resonant ODMR has an upper limit on the value of magnetic field that can be measured. When the external magnetic field is misaligned with the NV-center symmetry axis, the states with different spin projections intermix, which leads to lowered ODMR contrast and an overall drop in fluorescence levels [11]. As a result, conventional ODMR becomes less effective for off-axis fields higher than 100 G. However, the drop in the overall fluorescence level can be used to detect strong off-axis magnetic fields without using the MW radiation. This approach has been implemented in single centers [12], but in the ensemble case the changes in fluorescence levels can also be caused by spatial inhomogeneity of the NV-center distribution. Therefore, to measure spatially varying magnetic fields with arrays of NV centers a different protocol based on measuring spin relaxation contrast has been developed [13]. Another approach exploiting the properties of the ground-state-level anticrossing (GSLAC) of the NV center was suggested [14]. Though it does not require MW radiation, a strong and well-oriented magnetic field (1024 G) is necessary to observe a high-resolution GSLAC feature which limits potential applications.

In this paper we suggest another MW-free protocol that can be used to measure both the value and the orientation of the external magnetic field. The protocol is based on detecting cross-relaxation resonances that appear in the fluorescence when the magnetic field is scanned. These resonances are observed using resonant optical pumping on the NV-center zero phonon line. A room-temperature variant using off-resonant optical pumping is also briefly discussed.

II. THEORETICAL MODEL

The properties of NV centers change when they are cooled down to cryogenic temperatures. Below 35 K the resonant optical transitions are resolved, which divides the ensemble into four separate subgroups. The first subgroup consists of NV centers with optical transitions not resonant with the laser. This group is not affected by the optical excitation, so the ground-state sublevels are at equilibrium. The other three subgroups are characterized by the ground-state spin sublevel ($m_s = 0, \pm 1$) involved in the resonant optical transition. For these subgroups, the resonant excitation will burn spectral holes, transferring the population into other states, which leads to a decrease in fluorescence [15,16]. In the absence of spectral diffusion, this process is mostly limited by the ground-state spin relaxation. Without relaxation, the population would be completely transferred into the dark states and the fluorescence would be quenched. However, spin relaxation competes with the hole-burning process, leaving some of the population in the fluorescing states.

At cryogenic temperatures the ground-state relaxation process is dominated by spin-spin cross relaxation [17]. Dipole-dipole interaction between centers with equal ground-state transition frequencies leads to population exchange between them. If the ensembles of NV centers involved in this process are polarized differently (e.g., different subgroups formed

*rinat@appl.sci-nnov.ru

by the resonant optical excitation as discussed above), this additional population exchange can depolarize the ensembles, leading to an increase in fluorescence. NV centers can also be divided into four groups with different symmetry axis orientations that correspond to space diagonals of the crystal lattice cube. Without the external magnetic field all four groups have the same ground-state splitting, so all NV centers take part in cross relaxation, lowering the effective longitudinal spin-relaxation time T_1 and increasing fluorescence. An external magnetic field splits the ground states of the four groups differently, taking their ground-state transitions out of resonance with each other. As a result, the cross-relaxation rate becomes lower and the fluorescence decreases. However, certain orientations of the external magnetic field can split the ground states of different NV-center groups equally (i.e., accidental degeneracy). If the magnetic field is scanned around these orientations, resonances in the fluorescence level are observed.

Let us consider the case where the diamond sample is placed into an external magnetic field consisting of two components: the unknown constant field, $\vec{B}^{\rm dc}$, and an additional field, $\vec{B}^{\rm scan}$, with fixed orientation but adjustable value. When the value of the additional field is scanned, the fluorescence profile will display several resonances that correspond to external-field orientations with ground-state transition degeneracy.

To find the expected positions of these resonances, let us consider the ground-state splitting of the NV center in the external magnetic field $\vec{B}$. The frequencies of the ground-state transitions can be written as [16]

$$\nu_i = 2\sqrt{3}[(3k^2 + D^2)/9]^{\frac{1}{2}} \sin(\alpha/3 + \Delta_i), \tag{1}$$

where $\Delta_i = \pi/3, 2\pi/3$, and π correspond to the three possible ground-state transitions between the $m_s = 0$ and ± 1 sublevels, $k = g\mu_B B$, $D = 2.88$ GHz is the zero-field ground-state splitting, θ is the angle between the magnetic field and the defect symmetry axis, and α can be obtained from the equation

$$\cos\alpha = \frac{9Dk^2 - 27Dk^2\cos^2\theta + 2D^3}{2(3k^2 + D^2)^{\frac{3}{2}}}. \tag{2}$$

The transition frequencies of two different NV centers (denoted by indices 1 and 2) coincide when

$$|\sin(\alpha_1/3 + \Delta_i)| = |\sin(\alpha_2/3 + \Delta_j)|. \tag{3}$$

Cycling through different Δ_i and Δ_j (i.e., different ground-state transitions), we obtain the following conditions for α:

$$\alpha_1 = \pm\alpha_2(+\pi) \Rightarrow \cos\alpha_1 = \pm\cos\alpha_2. \tag{4}$$

The first case can be rewritten as

$$\cos\alpha_1 = \cos\alpha_2 \Rightarrow \cos^2\theta_1 = \cos^2\theta_2. \tag{5}$$

This condition corresponds to the case where the external magnetic field has equal projections onto the symmetry axes of two different NV-center groups, for example, when the external magnetic field lies in the bisecting plane of the angle formed by any two NV-center orientations.

For the magnetic field $\vec{B} = \vec{B}^{\rm dc} + \vec{B}^{\rm scan}$, the projections onto two different axes will be equal when

$$(\vec{B}^{\rm dc} + \vec{B}^{\rm scan}, \vec{e}_i) = \pm(\vec{B}^{\rm dc} + \vec{B}^{\rm scan}, \vec{e}_j), \quad i \neq j, \tag{6}$$

where $\{\vec{e}\} = [1, \pm 1, \pm 1]$ are the four vectors corresponding to the orientations of the symmetry axes of different NV-center groups.

These conditions can be rewritten as

$$(\vec{B}^{\rm dc} + \vec{B}^{\rm scan}, \vec{v}_k) = 0, \tag{7}$$

where $\{\vec{v}\} = \{\vec{e}_i \pm \vec{e}_j;\ i, j = \overline{1,4}\}$. These equations denote planes with normal vectors $\vec{v}_k$. While there are 12 possible combinations of $\vec{e}_i \pm \vec{e}_j$, three pairs of combinations correspond to the same vector. These three vectors define planes where two pairs of NV-center groups are simultaneously involved in cross relaxation. Overall, there are nine unique planes and nine conditions for cross-relaxation resonances.

Denoting $\vec{B}^{\rm scan} = B\vec{b}^{\rm scan}$, where $\vec{b}^{\rm scan}$ is the unitary vector and B is the value of the scanned field, we obtain nine values that correspond to cross-relaxation resonances:

$$B_i = -\frac{(\vec{B}^{\rm dc}, \vec{v}_i)}{(\vec{b}^{\rm scan}, \vec{v}_i)}. \tag{8}$$

Using coordinates tied to the crystallographic axes of the cubic lattice ($\vec{x} = [100]$, $\vec{y} = [010]$, $\vec{z} = [001]$), these resonances are given by

$$B_{[100]} = -\frac{B_x^{\rm dc}}{b_x^{\rm scan}}, \tag{9}$$

$$B_{[010]} = -\frac{B_y^{\rm dc}}{b_y^{\rm scan}}, \tag{10}$$

$$B_{[001]} = -\frac{B_z^{\rm dc}}{b_z^{\rm scan}}, \tag{11}$$

$$B_{[110]} = -\frac{B_x^{\rm dc} + B_y^{\rm dc}}{b_x^{\rm scan} + b_y^{\rm scan}}, \tag{12}$$

$$B_{[101]} = -\frac{B_x^{\rm dc} + B_z^{\rm dc}}{b_x^{\rm scan} + b_z^{\rm scan}}, \tag{13}$$

$$B_{[011]} = -\frac{B_y^{\rm dc} + B_z^{\rm dc}}{b_y^{\rm scan} + b_z^{\rm scan}}, \tag{14}$$

$$B_{[1\bar{1}0]} = -\frac{B_x^{\rm dc} - B_y^{\rm dc}}{b_x^{\rm scan} - b_y^{\rm scan}}, \tag{15}$$

$$B_{[10\bar{1}]} = -\frac{B_x^{\rm dc} - B_z^{\rm dc}}{b_x^{\rm scan} - b_z^{\rm scan}}, \tag{16}$$

$$B_{[01\bar{1}]} = -\frac{B_y^{\rm dc} - B_z^{\rm dc}}{b_y^{\rm scan} - b_z^{\rm scan}}. \tag{17}$$

Let us consider the second case given by Eq. (4), the opposite cosines:

$$\begin{aligned}\cos\alpha_1 = &-\cos\alpha_2 \Rightarrow 9Dk^2 - 27Dk^2\cos^2\theta_1 + 2D^3 \\ &= -(9Dk^2 - 27Dk^2\cos^2\theta_2 + 2D^3),\end{aligned} \tag{18}$$

$$\cos^2\theta_1 + \cos^2\theta_2 = \frac{2}{3} + \frac{4}{27}\frac{D^2}{k^2}. \tag{19}$$

Considering that in the same coordinate system the angle between the magnetic field and the defect symmetry axes

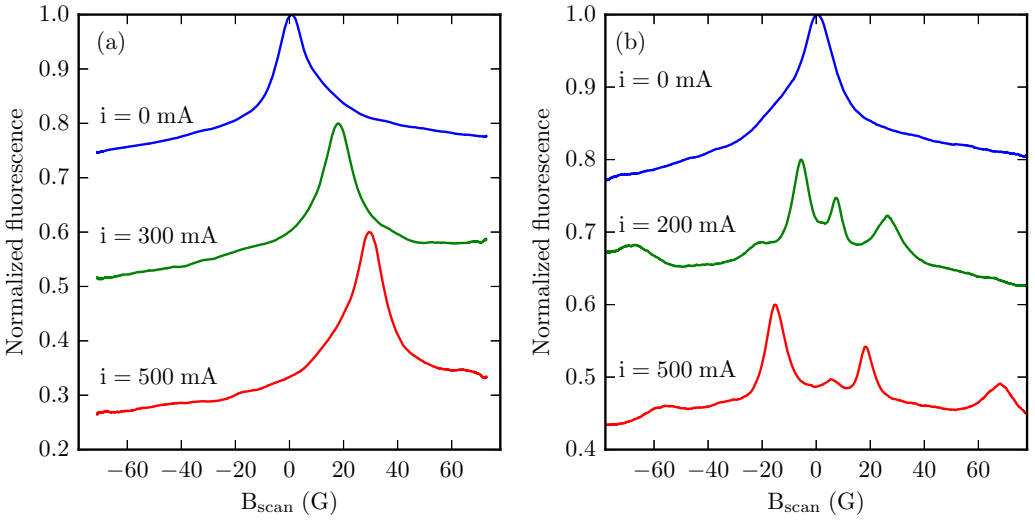

FIG. 1. Normalized fluorescence dependence on the value of the scanned field in the presence of an additional constant field $\vec{B}^{\rm dc}$ which is either parallel to the scanned field (a) or perpendicular to it (b). i denotes the current through the coil that generates $\vec{B}^{\rm dc}$. The graphs are offset for clarity.

can be written as $\cos\theta = \frac{B_x \pm B_y \pm B_z}{\sqrt{3}|B|}$, we obtain the following resonance conditions:

$$B_x B_y = \pm\left(\frac{B_{\rm LAC}}{3}\right)^2, \tag{20}$$

$$B_x B_z = \pm\left(\frac{B_{\rm LAC}}{3}\right)^2, \tag{21}$$

$$B_y B_z = \pm\left(\frac{B_{\rm LAC}}{3}\right)^2, \tag{22}$$

where $B_{\rm LAC} = \frac{D}{g\mu_B}$. One of the possible solutions is the well-researched resonance observed around 600 G ($\frac{B_{\rm LAC}}{\sqrt{3}}$) for the magnetic field along the [111] direction [16,18].

For the magnetic field $\vec{B} = \vec{B}^{\rm dc} + B\vec{b}^{\rm scan}$, we obtain the following 12 resonance conditions:

$$B^2 b_x^{\rm scan} b_y^{\rm scan} + B\left(B_y^{\rm dc} b_x^{\rm scan} + B_x^{\rm dc} b_y^{\rm scan}\right) + B_x^{\rm dc} B_y^{\rm dc} \pm (B_{\rm LAC}/3)^2 = 0, \tag{23}$$

$$B^2 b_x^{\rm scan} b_z^{\rm scan} + B\left(B_z^{\rm dc} b_x^{\rm scan} + B_x^{\rm dc} b_z^{\rm scan}\right) + B_x^{\rm dc} B_z^{\rm dc} \pm (B_{\rm LAC}/3)^2 = 0, \tag{24}$$

$$B^2 b_y^{\rm scan} b_z^{\rm scan} + B\left(B_z^{\rm dc} b_y^{\rm scan} + B_y^{\rm dc} b_z^{\rm scan}\right) + B_y^{\rm dc} B_z^{\rm dc} \pm (B_{\rm LAC}/3)^2 = 0. \tag{25}$$

III. EXPERIMENT

To confirm the validity of the model, we carry out an experiment aimed at observing the cross-relaxation resonances. We use a confocal microscopy setup [15]. A dye laser tuned to 637-nm wavelength is used to pump the NV centers. The diamond sample is prepared in the Lebedev Physical Institute using Element Six synthetic diamonds as the base. Those diamonds are irradiated by an electron beam (the radiation dose is 10^{18} electrons per square centimeter) and subsequently annealed at 800 °C. The sample is placed inside a coil that is used to create the scannable part of the external magnetic field $\vec{B}^{\rm scan}$. The sample and the coil are put inside the liquid helium cryostat where they are cooled down to 2 K. A second coil is placed outside the cryostat. This coil is used to create the "constant" part of the magnetic field $\vec{B}^{\rm dc}$. The diamond-sample fluorescence is transmitted through a longpass filter with the threshold around 650 nm to cut off the leftover laser radiation and then detected using a photomultiplier tube.

The fluorescence dependence on the value of the scanned field is shown in Fig. 1, while for the dc field there are two possible orientations, one of which is perpendicular to the scanned field and the other is parallel to it. As the orientation of the crystal axes of the sample is not known to us, the scanned field $\vec{B}^{\rm scan}$ is applied to the sample at some arbitrary angle. The fluorescence dependence shows a resonance with a peak at zero field. The width of the peak is around 10 G and the contrast is around 10%. A similar effect has been observed in the absorption profile at the zero phonon line for small values of the external magnetic field [16]. A similar feature in the fluorescence profile has also been observed for small magnetic fields at room temperature with off-resonant optical pump, but the contrast was significantly lower (<1%) [19].

As expected, applying an additional magnetic field $\vec{B}^{\rm dc}$ along the same direction as $\vec{B}^{\rm scan}$ shifts the scan as a whole [see Fig. 1(a)] and the size of the shift depends on the value of the additional field. In contrast, when the additional field is perpendicular to the scanned field, we observe several separate resonance peaks [see Fig. 1(b)]. We assume that each resonance peak corresponds to an increase in the cross-relaxation rate caused by overlapping of the ground-state transition frequencies for different groups of NV centers.

To confirm the assumption, we use optically resonant ODMR [15] to investigate the ground-state transition frequencies. The fluorescence dependence on the scanned magnetic field for a chosen value of the constant magnetic field $\vec{B}^{\rm dc}$ is

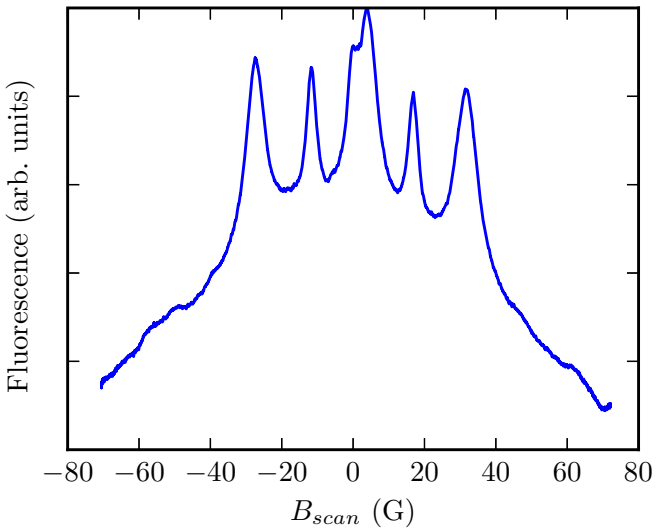

FIG. 2. NV-center fluorescence as a function of the scanned field value. The constant field $\vec{B}^{\rm dc}$ is perpendicular to the scanned field. The orientation of the crystal axes is different from the case shown in Fig. 1.

shown in Fig. 2. The constant magnetic field is perpendicular to the scanned field $\vec{B}^{\rm scan}$. The diamond crystal orientation used is different from that in Fig. 1. When the MW radiation is added to the external magnetic field, we observe additional resonance peaks on the fluorescence scans at magnetic fields where the MW radiation frequency coincides with one of the ground-state transitions. The experiment is repeated with different frequencies of MW radiation. The results are shown in Fig. 3. Each vertical stripe corresponds to a normalized fluorescence scan performed at the set MW frequency.

It can be seen that each resonance peak (bright horizontal lines in Fig. 3) corresponds to a crossing of ODMR curves belonging to different NV-center groups. This correspondence confirms that the resonances are caused by cross relaxation. Using the peak positions in Fig. 2 and Eqs. (9)–(17), it is possible to find the values of $B_x^{\rm dc}$, $B_y^{\rm dc}$, $B_z^{\rm dc}$, $b_x^{\rm scan}$, $b_y^{\rm scan}$, and $b_z^{\rm scan}$. However, as the actual orientation of the crystal axes relative to the scanned magnetic field is not known, these values can only be determined with an ambiguity determined by all possible NV-center group (or x, y, and z axes) permutations. The theoretical magnetic resonance positions that correspond to these magnetic field values are plotted in Fig. 3 by four pairs of lines. These lines demonstrate good agreement with the experimental measurements. Significantly, despite the ambiguity of the orientation of crystal axes, it is possible to obtain the exact value of the magnitude of the constant field $B^{\rm dc}$ (23 G) and its projection onto the scanned field direction (−0.15 G).

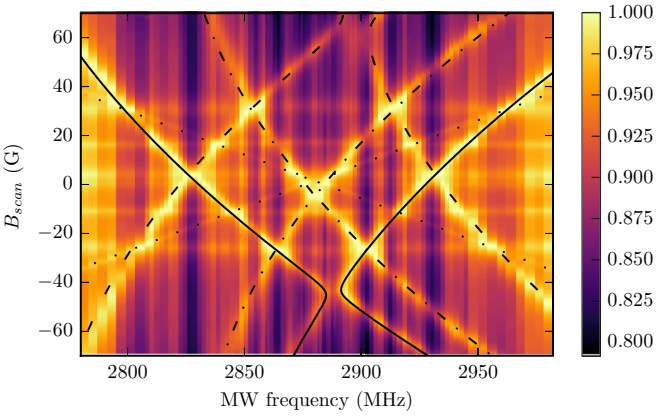

FIG. 3. Normalized fluorescence as a function of the MW radiation frequency and the scanned field value. The constant field $\vec{B}^{\rm dc}$ is perpendicular to the scanned field. Black lines show calculated transition frequencies for differently oriented NV-center groups. Four different line styles are used to distinguish between different groups.

These results show that the cross-relaxation resonances can be used to measure external magnetic fields. To determine all components of the magnetic field vector, it is necessary to know the exact orientation of the diamond crystal axes. In this case, it is possible to implement a simple magnetometry protocol.

IV. MAGNETOMETRY PROTOCOL

To illustrate the protocol, let us consider the case where the magnetic field is scanned along one of the crystallographic axes: $\vec{b}^{\rm scan} = \vec{x}$, $b_x^{\rm scan} = 1$, $b_y^{\rm scan} = 0$, and $b_z^{\rm scan} = 0$. Substituting these values into Eqs. (9)–(17), we obtain the following nine resonance values of the scanned magnetic field:

$$B_{[100]} = -B_x^{\rm dc}, \tag{26}$$

$$B_{[110]} = -\left(B_x^{\rm dc} + B_y^{\rm dc}\right), \tag{27}$$

$$B_{[1\bar{1}0]} = -\left(B_x^{\rm dc} - B_y^{\rm dc}\right), \tag{28}$$

$$B_{[101]} = -\left(B_x^{\rm dc} + B_z^{\rm dc}\right), \tag{29}$$

$$B_{[10\bar{1}]} = -\left(B_x^{\rm dc} - B_z^{\rm dc}\right), \tag{30}$$

$$B = -B_x^{\rm dc} \pm \left(\frac{B_{\rm LAC}}{3}\right)^2 \frac{1}{B_y^{\rm dc}}, \tag{31}$$

$$B = -B_x^{\rm dc} \pm \left(\frac{B_{\rm LAC}}{3}\right)^2 \frac{1}{B_z^{\rm dc}}. \tag{32}$$

The last four resonances correspond to the case where the external magnetic field has different projections onto two NV-center groups but leads to the same ground-state transition frequencies. For sufficiently small measured magnetic fields (< 300 G), these resonances require high values of the scanned magnetic field and do not need to be considered.

The position of the central resonance peak can be used to obtain the exact value of the $B_x^{\rm dc}$ component. Furthermore, the absolute value of the magnetic field and the absolute values of its projections onto the y and z axes can be determined from the positions of the four other resonances. However, $|B_y|$ and $|B_z|$ projections cannot be told apart in such a measurement.

Performing similar measurements with the magnetic field $B^{\rm scan}$ being scanned along the two other crystallographic axes, [010] and [001], we can determine the exact values of the $B_y^{\rm dc}$ and $B_z^{\rm dc}$ projections, respectively. These three measurements are sufficient to obtain complete information

about the unknown magnetic field $\vec{B}^{\rm dc}$. An important feature of the protocol is that, unlike conventional ODMR, it does not rely on measuring the exact value of the ground-state splitting so it is not dependent on temperature.

The suggested protocol has two limitations (similar to the vector ODMR magnetometer [20]). If the measured field is too weak, the resonance peaks cannot be separated due to their finite width. In this case, an additional field perpendicular to the scanned field direction can be used to split the resonances and determine the position of the central peak. The central peak position is not affected by the additional magnetic field so it still corresponds to the value of the measured magnetic field projection onto the scan axis. Another exception is the case where the measured magnetic field is oriented along [100], [010], or [001] axes (when off-axis components are sufficiently small). When the scanned field is codirectional with the measured magnetic field, the projections of the total magnetic field onto all four NV-center axes are equal, so the spin exchange rate is constant and no resonances will be observed on the fluorescence scan. If the scanned field is perpendicular to the measured field, the total magnetic field always lies in the plane where the projections onto two separate pairs of NV centers are equal. As a result, the fluorescence scan only has a resonance at zero scanned field independent of the applied field strength and this resonance gives no meaningful information about the values of the measured field components. An additional magnetic field perpendicular both to the measured field and to the scanned field can be used to remove the group degeneracy and measure the field components.

Let us estimate the sensitivity $\eta(\mathrm{T/Hz^{1/2}})$ of the suggested approach to magnetometry. Considering optical shot noise to be the main source of noise in the scheme, the sensitivity can be approximated using the formula $\eta = \frac{\Delta B}{C\sqrt{I_0}}$, where $\Delta B = 10$ G and $C = 0.1$ are the resonance width and contrast, respectively, and I_0 is the photon detection rate. The fluorescence intensity is proportional to the total quantity of NV centers in the sample and depends on the relaxation rate $\gamma = \frac{1}{T_1}$. The photon detection rate can be estimated as $I_0 = \frac{1}{T_1} N \eta_{\rm detect}$, where $\eta_{\rm detect} \simeq 0.01$ is the efficiency of fluorescence gathering and detection [4]. Only the centers affected by the laser contribute to the fluorescence, so the amount of NV centers can be estimated as $N = nV\frac{\Delta\nu_{\rm laser}}{\Delta\nu_{\rm inhom}}$, where n is the NV-center concentration, V is the affected volume, $\Delta\nu_{\rm laser}$ is the laser linewidth (which is limited by the splitting of the NV-center ground state), and $\Delta\nu_{\rm inhom}$ is the inhomogeneous zero phonon linewidth of the NV-center ensemble. For samples with high NV-center concentrations the typical values are $n = 40$ ppm $\simeq 7\times10^{18}\,\mathrm{cm^{-3}}$, $1/T_1 \simeq 10^3\,\mathrm{s^{-1}}$ [21], and $\Delta\lambda_{\rm inhom} \simeq 1$ nm (which corresponds to $\Delta\nu_{\rm inhom} \simeq 500$ GHz). For the $100\times100\times100\,\mu\mathrm{m}^3$ interaction volume and the laser linewidth close to 1 GHz, we obtain the detection rate $I_0 \simeq 1.4\times10^{11}\,\mathrm{s^{-1}}$. The resulting sensitivity can be estimated as $27\,\mathrm{nT/Hz^{1/2}}$.

The necessity of cryogenic cooling can be detrimental for practical applications. However, there is evidence indicating that dipole-dipole interaction between NV centers can affect fluorescence induced by off-resonant optical pumping at room temperature [17,19,21]. With that in mind, we perform an additional experiment at room temperature using a 532-nm green laser. The results are shown in Fig. 4. Similar to the case of resonant pumping at 2 K, resonances are observed when the magnetic field $\vec{B}^{\rm scan}$ is scanned with an additional constant magnetic field $\vec{B}^{\rm dc}$ present. From the ODMR data shown in Fig. 4 it can be seen that the resonances correspond to the field values where the transition frequencies of differently oriented NV-center groups overlap. However, unlike the resonant optical pumping case, the exact mechanism behind the fluorescence change remains unclear. While the contrast of resonances at room temperature is much lower than in the previous experiment ($C \simeq 0.01$), the sensitivity can be better due to a higher fluorescence rate. This is because the off-resonant pump interacts with all NV centers in the same way, so there is no hole burning and all NV centers contribute to fluorescence. As a result, the photon detection rate can be estimated as $I_0 = \frac{1}{T_{\rm opt}} nV\eta_{\rm detect}$, where $T_{\rm opt} \simeq 10^{-8}$ s is the excited-state lifetime. The resulting photon detection rate is $I_0 \simeq 7\times10^{18}\,\mathrm{s^{-1}}$ and the sensitivity is around $38\,\mathrm{pT/Hz^{1/2}}$ for the same interaction volume of $100\times100\times100\,\mu\mathrm{m}^3$.

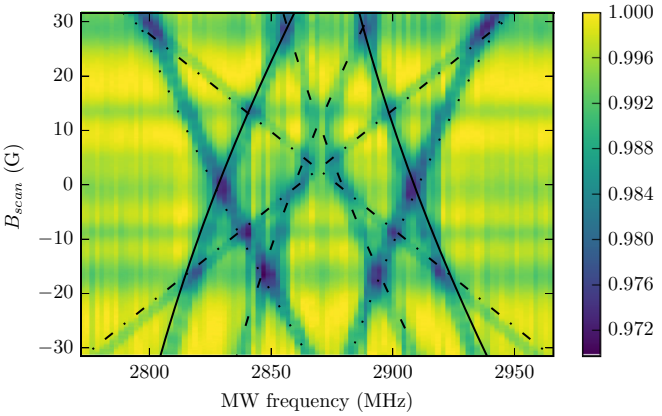

FIG. 4. Normalized fluorescence as a function of the MW radiation frequency and the scanned field value. An off-resonant green pump at room temperature is used to induce the fluorescence. The constant field $\vec{B}^{\rm dc}$ is perpendicular to the scanned field. Black lines show calculated transition frequencies for differently oriented NV-center groups. Four different line styles are used to distinguish between different groups.

V. CONCLUSION

In this paper we observe cross-relaxation resonances between differently oriented groups of NV centers at small external magnetic fields. We suggest a magnetometry protocol that is based on measuring the positions of cross-relaxation resonances on the fluorescence scan. This protocol does not require MW radiation and can be used to find all components of the unknown magnetic field vector.

ACKNOWLEDGMENTS

We are grateful to V. L. Velichansky and A. O. Levchenko for the diamond samples. The work was performed as part of the State Assignment of the Institute of Applied Physics RAS, Project No. 0035-2014-0005.

[1] M. V. G. Dutt, L. Childress, L. Jiang, E. Togan, J. Maze, F. Jelezko, A. S. Zibrov, P. R. Hemmer, and M. D. Lukin, Science **316**, 1312 (2007).

[2] S. Kolkowitz, A. C. B. Jayich, Q. P. Unterreithmeier, S. D. Bennett, P. Rabl, J. G. E. Harris, and M. D. Lukin, Science **335**, 1603 (2012).

[3] G. Kucsko, P. C. Maurer, N. Y. Yao, M. Kubo, H. J. Noh, P. K. Lo, H. Park, and M. D. Lukin, Nature (London) **500**, 54 (2013).

[4] J. M. Taylor, P. Cappellaro, L. Childress, L. Jiang, D. Budker, P. R. Hemmer, A. Yacoby, R. Walsworth, and M. D. Lukin, Nat. Phys. **4**, 810 (2008).

[5] G. Balasubramanian, I. Y. Chan, R. Kolesov, M. Al-Hmoud, J. Tisler, C. Shin, C. Kim, A. Wojcik, P. R. Hemmer, A. Krueger, T. Hanke, A. Leitenstorfer, R. Bratschitsch, F. Jelezko, and J. Wrachtrup, Nature (London) **455**, 648 (2008).

[6] J. R. Maze, P. L. Stanwix, J. S. Hodges, S. Hong, J. M. Taylor, P. Cappellaro, L. Jiang, M. V. G. Dutt, E. Togan, A. S. Zibrov, A. Yacoby, R. L. Walsworth, and M. D. Lukin, Nature (London) **455**, 644 (2008).

[7] L. M. Pham, D. Le Sage, P. L. Stanwix, T. K. Yeung, D. Glenn, A. Trifonov, P. Cappellaro, P. R. Hemmer, M. D. Lukin, H. Park, A. Yacoby, and R. L. Walsworth, New J. Phys. **13**, 045021 (2011).

[8] L. Thiel, D. Rohner, M. Ganzhorn, P. Appel, E. Neu, B. Muller, R. Kleiner, D. Koelle, and P. Maletinsky, Nat. Nanotechnol. **11**, 677 (2016).

[9] M. Pelliccione, A. Jenkins, P. Ovartchaiyapong, C. Reetz, E. Emmanouilidou, N. Ni, and A. C. B. Jayich, Nat. Nanotechnol. **11**, 700 (2016).

[10] D. M. Toyli, D. J. Christle, A. Alkauskas, B. B. Buckley, C. G. Van de Walle, and D. D. Awschalom, Phys. Rev. X **2**, 031001 (2012).

[11] J.-P. Tetienne, L. Rondin, P. Spinicelli, M. Chipaux, T. Debuisschert, J.-F. Roch, and V. Jacques, New J. Phys. **14**, 103033 (2012).

[12] L. Rondin, J.-P. Tetienne, P. Spinicelli, C. D. Savio, K. Karrai, G. Dantelle, A. Thiaville, S. Rohart, J.-F. Roch, and V. Jacques, Appl. Phys. Lett. **100**, 153118 (2012).

[13] D. A. Simpson, J.-P. Tetienne, J. M. McCoey, K. Ganesan, L. T. Hall, S. Petrou, R. E. Scholten, and L. C. L. Hollenberg, Sci. Rep. **6**, 22797 (2016).

[14] A. Wickenbrock, H. Zheng, L. Bougas, N. Leefer, S. Afach, A. Jarmola, V. M. Acosta, and D. Budker, Appl. Phys. Lett. **109**, 053505 (2016).

[15] R. Akhmedzhanov, L. Gushchin, N. Nizov, V. Nizov, D. Sobgayda, I. Zelensky, and P. Hemmer, Phys. Rev. A **94**, 063859 (2016).

[16] K. Holliday, N. B. Manson, M. Glasbeek, and E. van Oort, J. Phys.: Condens. Matter **1**, 7093 (1989).

[17] A. Jarmola, V. M. Acosta, K. Jensen, S. Chemerisov, and D. Budker, Phys. Rev. Lett. **108**, 197601 (2012).

[18] E. van Oort and M. Glasbeek, Phys. Rev. B **40**, 6509 (1989).

[19] S. V. Anishchik, V. G. Vins, A. P. Yelisseyev, N. N. Lukzen, N. L. Lavrik, and V. A. Bagryansky, New J. Phys. **17**, 023040 (2015).

[20] A. K. Vershovskii and A. K. Dmitriev, Tech. Phys. Lett. **41**, 393 (2015).

[21] M. Mrozek, D. Rudnicki, P. Kehayias, A. Jarmola, D. Budker, and W. Gawlik, EPJ Quantum Technol. **2**, 22 (2015).